A Master-Slave System Using a Multi-DOF Ultrasonic Motor and its Controller Designed Considering Measured and Simulated Driving Characteristics

Kenjiro TAKEMURA*, Dai HARADA**, and Takashi MAENO**

* Graduate School of Science and Technology, Keio University
3-14-1, Hiyoshi, Kohoku-ku, Yokohama, 223-8522 JAPAN
e-mail; kenjiro@mmm-keio.net

** Department of Mechanical Engineering, Keio University
3-14-1, Hiyoshi, Kohoku-ku, Yokohama, 223-8522 JAPAN
e-mail; haradai@aurora.dti.ne.jp, maeno@mech.keio.ac.jp

Abstract

Master-slave active robot hands and endoscopes, which provide dexterous manipulations and wide views like human hands and eyes, are required to be constructed. We have previously developed a multi-DOF ultrasonic motor consisting of a spherical rotor and a bar-shaped stator. The rotor rotates around three perpendicular axes using three natural vibration modes of the stator. In this study, a multi-DOF unilateral master-slave system using the multi-DOF ultrasonic motor is developed. Master and slave arms for the system have similar configurations, so that an operator can easily handle the master-slave system. First, driving characteristics of the multi-DOF ultrasonic motor are clarified experimentally and analytically in order to design the slave arm and its controller. Next, the master-slave arms and the unilateral feedback controller for the master-slave system are developed. Finally, the motion control tests of the system are performed to show the applicability of the master-slave system.

1. Introduction

As it is required for robots to be used in situations such as the universe or the surgical operation, needs for master-slave systems are extended, because such situations are harsh or particular for human. In other words, master-slave active robot hands and master-slave active endoscopes, which move like human hands and eyes, are required for effective robotics. Namely, the number of DOF of motion for the master and slave robots should be the same as, or more than that of human hands and eyes [1-3].

In order to provide equivalent dexterous motion, multi-DOF actuators are thought to have advantages in their volumes and weights compared with combinations of single-DOF electromagnetic motors. Roth *et al*. proposed a three-DOF variable reluctance spherical wrist motor [4], and Yano developed a spherical stepping motor [5]. Their motors use the principle of the electromagnetic motor, and thus, geometries of the motors are complicated.

On the other hand, ultrasonic motors have excellent characteristics such as high torque at low speed, high stationary limiting torque, absence of electromagnetic radiation, quiet, and simplicity of design. Therefore, multi-DOF actuators extending the principle of ultrasonic motors have been proposed as follows: Bansevicius developed a piezoelectric multi-DOF actuator [6]. Amano *et al*. developed a multi-DOF ultrasonic actuator [7]. Toyama constructed a spherical ultrasonic motor [8]. Sasae *et al*. developed a spherical actuator [9]. Although the actuators [6-9] can generate multi-DOF motions of rotors, they cannot be used in place of multi-DOF motion units consisting of general electromagnetic motors. This is due to the several reasons: First, a method for controlling the rotors in desired direction is not constructed. Second, their output torque are not large enough. Third, their configurations are complex. In order to solve these issues, the geometries of multi-DOF ultrasonic motors must be precisely designed and their driving characteristics should be theoretically clarified.

In our earlier studies, the authors have developed a new type of ultrasonic motor capable of generating multi-DOF motion [10]. The multi-DOF ultrasonic motor generates multi-DOF rotation of a spherical rotor using three natural vibration modes of a bar-shaped stator. The ultrasonic motor can generate motion similar to the human wrist using only one stator. Hence, a high-performance master-slave system can be constructed using the multi-DOF ultrasonic motor. In this study, a master-slave system using the multi-DOF ultrasonic motor and its controller are developed considering measured and analyzed driving characteristics of the multi-DOF ultrasonic motor.

Measured driving characteristics of the multi-DOF ultrasonic motor are briefly described in chapter 2. Then, a new type of simulation method for the multi-DOF ultrasonic motor is proposed for clarifying its driving characteristics. In chapter 3, a configuration of the master-slave system and its controller are described. Motion control tests are performed in chapter 4. Finally in chapter 5, the conclusions of this study are described.

2. Driving Characteristics of Multi-DOF Ultrasonic Motor

The multi-DOF ultrasonic motor we developed is shown in Fig. 1. The *x*-, *y*- and *z*-coordinate used in the present paper are defined as shown in Fig. 1. The diameter, length, and weight of a bar-shaped stator are 10 mm, 31 mm, and 16.9 g, respectively. Stacked PZT rings are used for exciting the natural vibrations on the stator. A spherical rotor is rotated around three perpendicular axes using a rotor/stator frictional force. When rotated around the *z*-axis, second bending modes in the *z*-*x* and *y*-*z* plane (B2_*x* and B2_*y*) of the stator are combined as shown in Fig. 2 (a). When rotated around the *x*- (*y*-) axis, a first longitudinal mode (L1_*z*) and second bending modes in the *y*-*z* (*z*-*x*) plane are combined as shown in Fig. 2 (b) [10].

2.1. Experimental Characteristics

In case of the multi-DOF ultrasonic motor, the frequency, voltage and phase of three input alternative signals for exciting each vibration mode have potentials for the operating parameter. The relationships between the each input parameter and rotational speed around the *x*-axis are shown in Fig. 3. The positive and negative values of the rotational speed correspond to the rotational direction, CW and CCW, respectively. Operating parameters for Fig. 3 (a), (b), and (c) are the frequency, input voltage for the second bending mode, and phase for the second bending mode, respectively. The pre-load between the rotor/stator is 4 N, and the other basic input parameters are as shown in Table 1. The voltage of input signal for the first longitudinal mode is fixed at 10 V, because the longitudinal mode is mainly used as a clutch and does not provide much driving force.

The rotational speed can be varied by changing the values of each parameter (Fig. 3). However, the rotational speeds vary non-linearly when the frequency and phase are changed. In case of Fig. 3 (b), the rotor does not stop when the voltage input for the second bending mode is 0 V, because the contact points between the rotor/stator do not vibrate exactly along the *z*-axis when the first longitudinal mode is only excited on the stator. Moreover, it can be seen that the rotational direction of the rotor can be reversed only when the sign of phase is changed.

The relationship between torque and rotational speed is shown in Fig. 4. The maximum torque and rotational speed are about 7 mNm and 250 rpm, respectively.

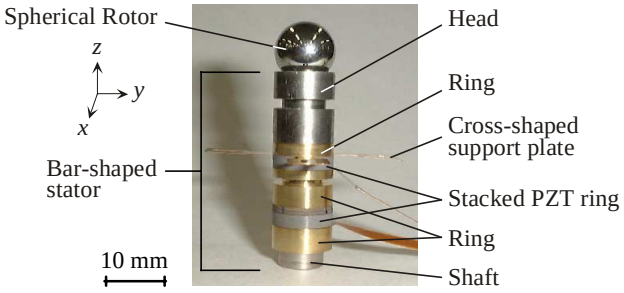

Fig. 1 The multi-DOF ultrasonic motor

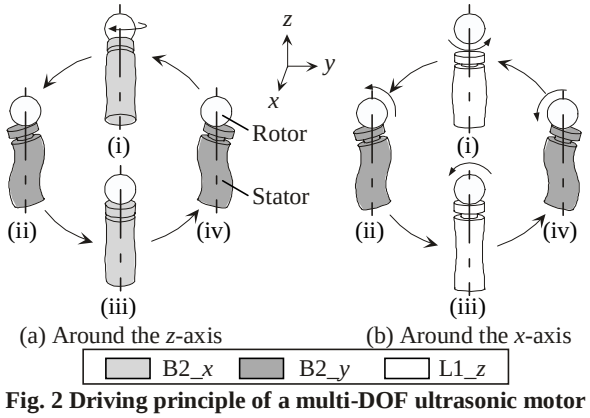

Fig. 2 Driving principle of a multi-DOF ultrasonic motor

2.2. Simulated Characteristics

(a) Simulation method

Only the simulation methods for obtaining

Table 1 Basic input for the multi-DOF ultrasonic motor

	Longitudinal mode	Bending mode in *z*-*x* plane
Voltage [V]	10	20
Phase [deg]	0	90
Freq. [kHz]	39.5	

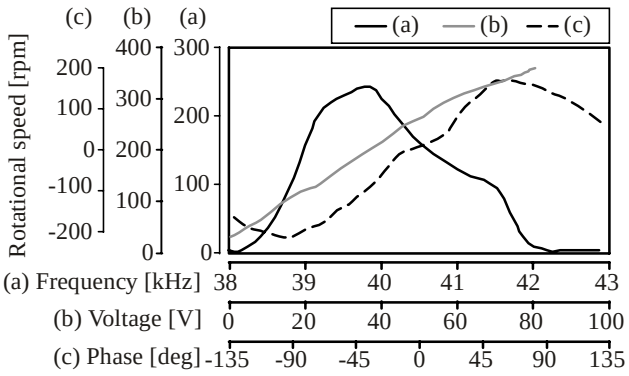

Fig. 3 Measured driving characteristics

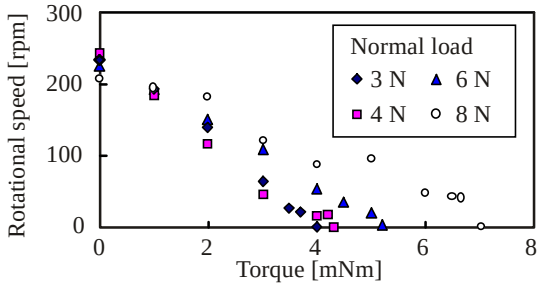

Fig. 4 Relationship between torque and rotational speed

characteristics of single-DOF ultrasonic motors have previously been developed [11][12]. So, a new type of numerical simulation method must be proposed to clarify the driving characteristics of the multi-DOF ultrasonic motor precisely.

As the ultrasonic motors are frictionally driven motor, the contact conditions between the rotor/stator are important for explaining their characteristics. So, the rotor/stator contact area is modeled using nodes P_i and liner springs k_i as shown in Fig. 5, where n is a total number of the nodes. The directions of each spring k_i are the same as those of vector $\boldsymbol{CP_i}$. A cycle of vibration is divided to m steps. A simulation method is proposed as follows.

First, the position of the center of rotor is calculated considering the balance of spring force and external pre-load between the rotor/stator. Then, positions $\boldsymbol{P}_{i,j}$ and velocities $\boldsymbol{v}_{i,j}$ of each node at each step are calculated using the shapes of each vibration modes obtained by the finite element analysis. i and j represent the numbers of node and step, respectively.

Second, driving torque $\boldsymbol{\tau}_{i,j}$ of each node at each step are obtained using the positions $\boldsymbol{P}_{i,j}$ and velocities $\boldsymbol{v}_{i,j}$ as follows. Kinematics' vectors at step j with regard to the rotor and node P_i are shown in Fig. 6, where $\boldsymbol{Axis}_{i,j}$ is a rotational axis by the torque $\boldsymbol{\tau}_{i,j}$, $\boldsymbol{\delta}_{i,j}$ is the decline of node P_i against the rotor, and $\boldsymbol{f}^{k}_{i,j}$ is the spring force. If it is assumed that the rotor is stationary and the stator always slips against the rotor, the node P_i provides a frictional force $\mu \boldsymbol{f}^{k}_{i,j}$ in the direction of velocity $\boldsymbol{v}_{i,j}$, where μ is a dynamic friction coefficient. Then, the torque $\boldsymbol{\tau}_{i,j}$ is defined by

$$\boldsymbol{\tau}_{i,j} = \mu \boldsymbol{f}^{k}_{i,j} \times \boldsymbol{CP}_{i,j} = \mu \boldsymbol{k}_i \boldsymbol{\delta}_{i,j} \times \boldsymbol{CP}_{i,j} \qquad (1)$$

A driving torque $\boldsymbol{T}$ of all nodes during a cycle is obtained as a summation of an average torque at each step. Then, the direction and magnitude of torque $\boldsymbol{T}$ represent the direction of the rotational axis and the maximum torque of the rotor, respectively.

Finally, the rotational speed, output torque and efficiency around the rotational axis derived above are calculated. If the rotational speed ω is known, an output torque $\tau^{out}_{i,j}$ and a power loss by friction $w^{loss}_{i,j}$ is defined by

$$\tau^{out}_{i,j} = \mu f^{k}_{i,j} \cdot \left| \frac{v^{t}_{i,j}}{v_{i,j}} \right| \cdot R_{i,j} \cdot \mathrm{sgn}\left(v^{t}_{i,j} - \omega R_{i,j} \right) \qquad (2)$$

$$w^{loss}_{i,j} = \mu f^{k}_{i,j} \cdot \left| \frac{v^{t}_{i,j}}{v_{i,j}} \right| \cdot \left| v^{t}_{i,j} - \omega R_{i,j} \right| \qquad (3)$$

where, $v^{t}_{i,j}$ and $R_{i,j}$ are a tangential velocity around the rotational axis and a distance from the rotational axis of node P_i, respectively. A total output torque T^{out} and a total power loss by friction W^{loss} are obtained as a summation of the average output torque and the power loss by friction at each step. Efficiency is calculated by

$$\eta = \frac{T^{out} \cdot \omega}{T^{out} \cdot \omega + W^{loss}} \qquad (4)$$

(b) Simulated results

Driving characteristics of the multi-DOF ultrasonic motor are calculated using the proposed method. The numbers of nodes, steps, and natural frequencies of the modes are 360, 100, and 40 kHz, respectively. Other analytical conditions and simulated results are shown in Table 2, where the rotational axes are normalized. When the two bending mode are combined, the rotational axis agrees with the z-axis, and when the longitudinal mode and the bending mode in the z-x plane are combined, it

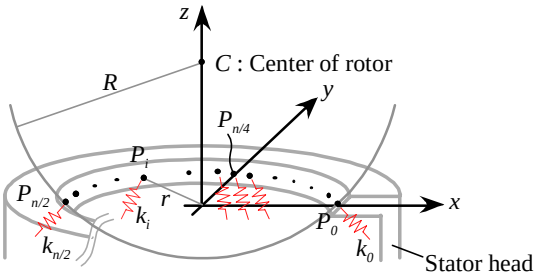

Fig. 5 Numerical model for multi-DOF ultrasonic motor

Table 2 Simulated conditions and results

No.		B2_x	B2_y	L1	Rot. axis	Rot. speed [rpm]
(1)	Amp. [μm]	1	1	0	$\begin{pmatrix}0\\0\\1\end{pmatrix}$	504
	Phase [deg]	0	90	0		
(2)	Amp. [μm]	1	0	1	$\begin{pmatrix}0\\1\\0\end{pmatrix}$	361
	Phase [deg]	0	0	90		
(3)	Amp. [μm]	1	0.8	1	$\begin{pmatrix}-0.422\\0.741\\-0.523\end{pmatrix}$	314
	Phase [deg]	0	30	60		

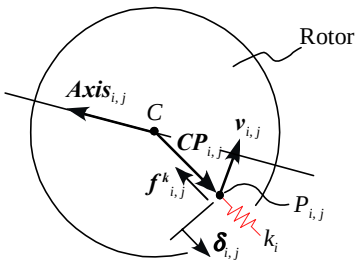

Fig. 6 Node P_i and its kinematics' vectors

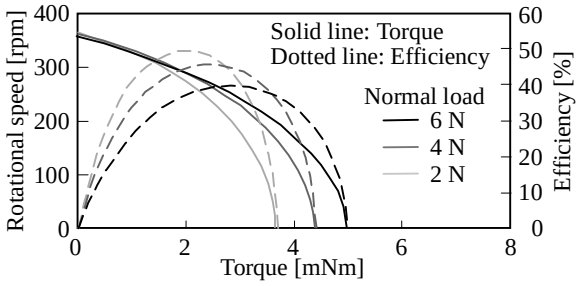

Fig. 7 Simulated driving characteristics

agrees with the *y*-axis as shown in Table 2 (1) and (2). The results agree well with the theoretical driving axis as shown in Fig.2. A rotational axis obtained in condition (3) means that the mixture of vibration modes occurred when phase differences of each modes are not equal to 0 or 180 deg.

Furthermore, simulated relationships between the output torque and rotational speed are shown in Fig. 7. It is seen from Fig. 7 that the rotational speed decreases as the torque increases, and that the efficiency shows a parabola characteristic. The maximum torque under the simulated conditions is about 5 mNm. The result agrees with the experimental results shown in Fig. 4.

Therefore, from Table 2, Fig. 4 and Fig. 7, the proposed method is confirmed to be numerically appropriate.

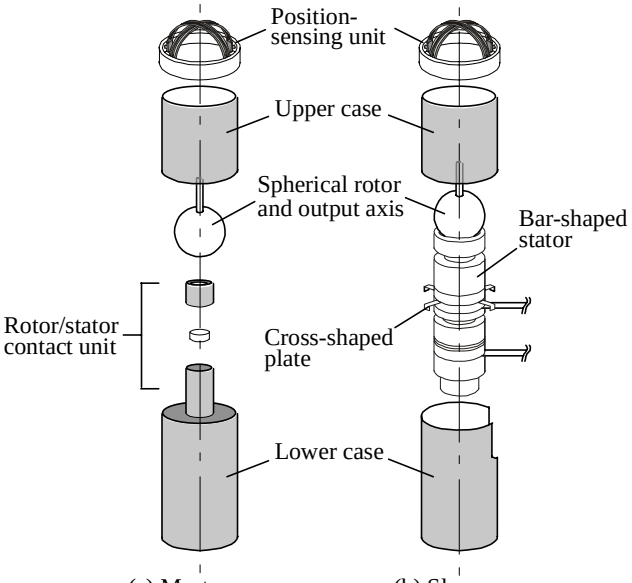

Fig. 8 Configurations of master and slave arms

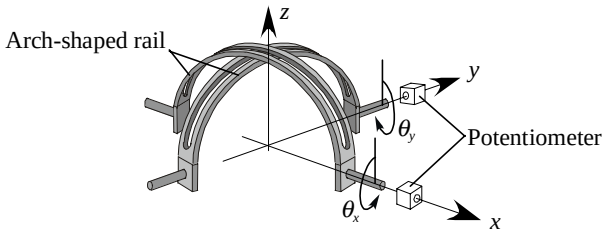

Fig. 9 Position sensing unit

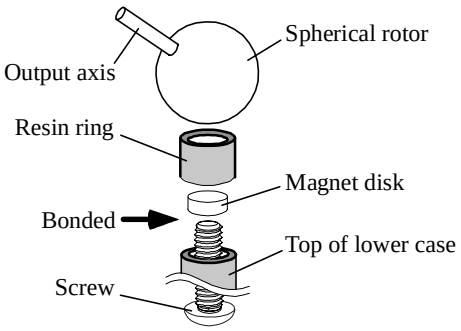

Fig. 10 Rotor/stator contact unit

3. Master-Slave System

3.1. Configuration

Multi-DOF master and slave arms using an above mentioned multi-DOF ultrasonic motor were then designed. Fig. 8 shows the configuration of the designed master and slave arms. The master arm consists of a position-sensing unit, a spherical rotor, a rotor/stator contact unit and cylindrical outer cases. The slave arm consists of the position-sensing unit, the multi-DOF ultrasonic motor and cylindrical outer cases. The multi-DOF ultrasonic motor is supported by a cross-shaped plate, which is held between the upper/lower cases. The position-sensing unit in detail is shown in Fig. 9. The unit has two potentiometers and two arch-shaped rails. Using the unit, angular positions of the spherical rotor around the *x*- and *y*-axis can be measured. The unit is located at the top of the upper case. The rotor/stator contact unit in detail is shown in Fig. 10. The spherical rotor is placed onto a resin ring, in which a magnet disk is located. The normal load between the rotor/stator can be adjusted by moving the magnet's position determined by a screw. The produced master and slave arms are shown in Fig. 11. The diameters and heights of both the master and slave arms are 15 mm and 44.5 mm, respectively.

As shown in Fig. 8 and Fig. 11, the configurations of

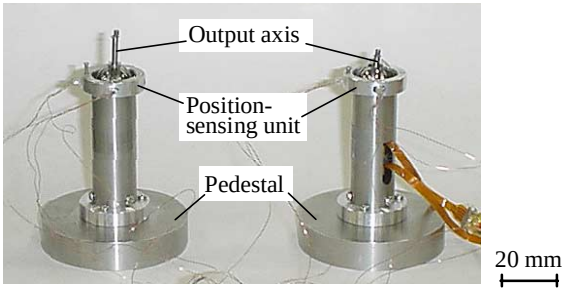

Fig. 11 Master and slave arms

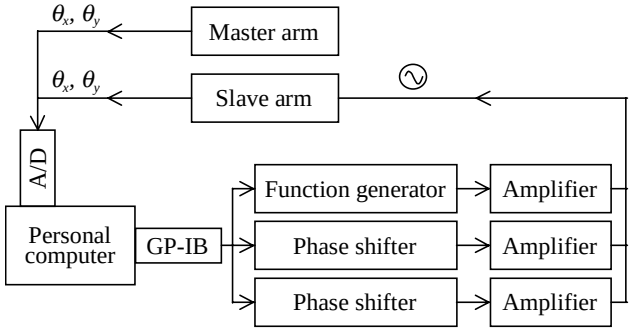

Fig. 12 Master-slave system

master and slave arms, especially for the position sensing unit and spherical rotor, are quite similar, so that they can be easily operated and their postures are easily identified.

The master-slave system is constructed as shown in Fig. 12. The angular positions of output axes obtained using potentiometers are input to a personal computer through an A/D converter. The three input signals for the multi-DOF ultrasonic motor are generated by a function generator and phase shifters, according to the declinations of angular positions.

3.2. Controller

First, we determined the operating parameter for the multi-DOF ultrasonic motor. All the parameters of input signals seem to have the potential to be the operating parameter as mentioned in section 2.1. Although frequency is usually used as the operating parameter in modern single-DOF ultrasonic motors, we adopt the voltage as the operating parameter because of the particular requirements such as,

(1) The rotational speeds around each axis must be controlled independently.
(2) There must not be an inappropriate mixture of vibration modes.

The frequency does not meet requirement (1) because the frequencies of the three input signals must be the same. As for requirement (2), if the phases are adopted as the operating parameter, there can be an inappropriate mixture of vibrations as seen in Table 2. Thus, the input voltages for the bending modes are suitable as the operating parameter. However, the rotational directions of the rotor should be controlled by the sign of time phases for bending vibrations.

Second, the control algorithm for the master-slave system is proposed. The proportional control method modified to add a bias component is used to control the voltages of the input signals as

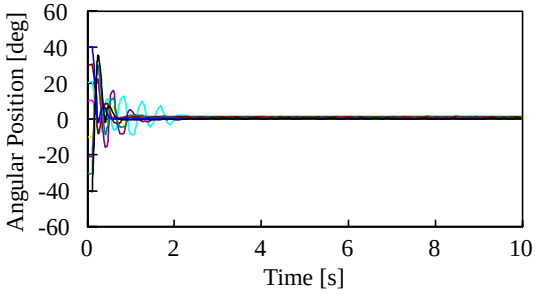

Fig. 13 Result for step response

Table 3 Experimental conditions for master-slave control tests

Experiment No.	Feedback gain K_p	Bias ε	Freq. [kHz]
(1)	0.10	0.00	39.11
(2)	0.10	0.30	39.11

$$V_{\xi'}^{ben} = K_p \cdot \left| \theta_{\xi}^{slave} - \theta_{\xi}^{master} \right| + \varepsilon \tag{5}$$

where, ξ and ξ' mean the coordinates, x (y) and y (x), respectively. $V_{\xi'}^{ben}$ is the input voltage for bending vibration in the ξ' direction, K_p is the proportional feedback gain, θ_{ξ}^{slave} and θ_{ξ}^{master} are the angular positions of spherical rotor around the ξ-axis for the slave and master arms, respectively, and ε is the bias. The reason why we adopt the bias is as follows. In case of ultrasonic motors, the rotor cannot be rotated when the amplitude of vibrations are too small because there is a pre-load between the rotor/stator with particular stiffness at their contact points. The phases of the input signals are determined as

$$\phi_{\xi'}^{ben} = \begin{cases} \pi/2 & (\theta_{\xi}^{slave} \geq \theta_{\xi}^{master}) \\ -\pi/2 & (\theta_{\xi}^{slave} \leq \theta_{\xi}^{master}) \end{cases} \tag{6}$$

where, $\phi_{\xi'}^{ben}$ is the phase of input signals for the bending vibrations in the ξ' direction. Then the controller for master-slave system was constructed using the algorithm mentioned above using Microsoft Visual C++.

4. Motion Control Tests

4.1. Step Response

Step responses of the rotor around the x-axis are tested first. A desired position is set at 0 deg, and initial positions are -40, -30, -20, -10, 10, 20, 30 and 40 deg. Fig. 13 shows the results for the step responses using the

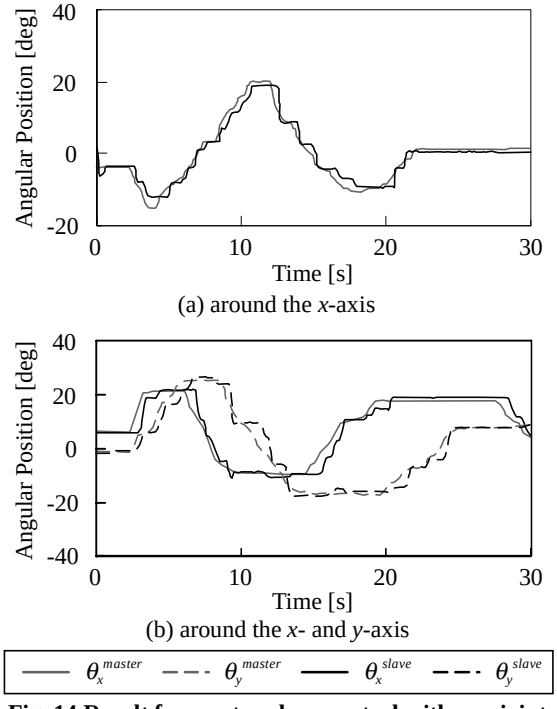

Fig. 14 Result for master-slave control with one joint

proportional controller when both the proportional feedback gain and bias are 0.1. Other experimental conditions follow those of Table 1.

It can be seen in Fig. 13 that the angular position of rotor is successfully controlled to the desired one using the proportional controller when the proportional feedback gain and bias are adjusted to suitable ones.

4.2. Control test of the Master-Slave System

Motion control tests of the master-slave system were conducted next. The experimental conditions are shown in Table 3. Experiment (1) is a control of angular position of the rotor only around the *x*-axis using the proportional controller. Angular positions around the *x*- and *y*-axis are controlled in parallel in experiment (2).

Fig.14 (a) shows the result for experiment (1). The angular position of the slave arm around the *x*-axis follows that of the master arm, although there remain some declinations of angular position.

Fig. 14 (b) shows the result for experiment (2). The angular positions of the slave arm around the *x*- and *y*-axis are controlled simultaneously to those of the master arm.

The values of proportional feedback gains and biases for the above experiments differ each other because there are differences of load torque and vibration characteristics for each experimental state. Although the rotor positions are controlled using the proposed controller, the oscillations of positions and the time delay for the motion of slave arm against that of master arm are seen in the Fig. 14. Errors are due to the rough sampling rate for the prototype system. However, it can easily be improved if an exclusive electronic circuit is produced for driving.

5. Conclusions

The master-slave system using the multi-DOF ultrasonic motor and its controller have been successfully developed.

First, a new type of simulation method for obtaining the driving characteristics of multi-DOF ultrasonic motor is proposed. Next, considering the measured and analyzed characteristics, the master-slave system is designed and constructed whose master and slave arms have similar configurations. The similar configurations of the master and slave arms are intended to provide an easy operation. Then the controller for the master-slave system is developed considering the characteristics of the multi-DOF ultrasonic motor. Finally, the motion control tests of the master-slave system are performed. The position of spherical rotor for the slave arm successfully follows that for the master arm using the developed controller.

A CCD camera should be mounted in the spherical rotor for the slave arm in a future study in order to confirm a practical possibility of the system. Future study is also focused on constructing a master-slave system that has a number of multi-DOF ultrasonic motors in series.

References

[1] K. Ikuta *et al.*, "Study on Hyper Endoscope for Remote Minimal Invasive Surgery," *Proc. 17th RSJ*, No. 2, pp. 675-676, 1999. [*in Japanese*]

[2] S. Guo *et al.*, "Micro Active Guide Wire Catheter System – Characteristic Evaluation, Electrical Model and Operability Evaluation of Micro Active Catheter -," *Proc. IEEE 6th Int. Symp. Micro Machine and Human Science*, pp. 131-136, 1995.

[3] S. Maeda *et al.*, " Micro Actuator with Shape Memory Alloy (SMA) Coil Spring and their Application to Active Fiberscopes," *IEICE Trans. Electronic*, Vol. E80-C, No. 2, pp. 226-231, 1997.

[4] R. Roth, and K-M. Lee, "Design Optimization of a Three Degrees-of-Freedom Variable Reluctance Spherical Wrist Motor," *Trans. ASME J. Engineering for Industry*, Vol. 117, pp. 378-388, 1995.

[5] T. Yano *et al.*, "Basic Characteristics of the Developed Spherical Stepping Motor," *Proc. 1999 IEEE/RSJ Int. Conf. Intelligent Robots and Systems*, Vol. 3, pp. 1393-1398, 1999.

[6] R. Bansevicius, "Piezoelectric Multi-degree of Freedom Actuators/Sensors," *Proc. 3rd Int. Conf. Motion and Vibration Control*, pp. K9-K15, 1996.

[7] T. Amano *et al.*, "An Ultrasonic Actuator with Multi-Degree of Freedom using Bending and Longitudinal Vibrations of a Single Stator," *Proc. IEEE Int. Ultrasonics Symp.*, pp.667-670, 1998.

[8] S. Toyama *et al.*, "Multi degree of freedom Spherical Ultrasonic Motor," *Proc. IEEE Int. Conf. Robotics and Automation*, pp. 2935-2940, 1995.

[9] K. Sasae *et al.*, "Development of a Small Actuator with Three Degrees of Rotational Freedom (3rd report)," *J. Japan Society of Precision Engineering*, Vol. 62, No. 4, pp. 599-603, 1996. [*in Japanese*]

[10] K. Takemura and T. Maeno, "Characteristics of an Ultrasonic Motor Capable of Generating a Multi-Degrees of Freedom Motion," *Proc. IEEE Int. Conf. Robotics and Automation*, pp. 3660-3665, 2000.

[11] T. Maeno *et al.*, "Finite Element Analysis of the Rotor/Stator Contact in Ring-Type Ultrasonic Motor," *IEEE Trans. Ultrasonic Ferroelectrics and Frequency Control*, Vol. 39, No. 6, pp. 668-674, 1992.

[12] T. Maeno, "Contact analysis of traveling wave type ultrasonic motor considering stick/slip condition," *J. the Acoustical Society of Japan*, Vol. 54, No. 4, pp. 305-311, 1998. [*in Japanese*]